

Article

Discrete-Time Quantum Walk on Multilayer Networks

Mahesh N. Jayakody ^{1,*}, Priodyuti Pradhan ², Dana Ben Porath ¹ and Eliahu Cohen ¹¹ Faculty of Engineering and the Institute of Nanotechnology and Advanced Materials, Bar-Ilan University, Ramat Gan 5290002, Israel; dana9494@gmail.com (D.B.P.); eliahu.cohen@biu.ac.il (E.C.)² networks.ai Lab, Department of Computer Science and Engineering, Indian Institute of Information Technology Raichur, Raichur 584135, Karnataka, India; priodyutipradhan@gmail.com

* Correspondence: jadmn.jayakody@gmail.com

Abstract: A Multilayer network is a potent platform that paves the way for the study of the interactions among entities in various networks with multiple types of relationships. This study explores the dynamics of discrete-time quantum walks on a multilayer network. We derive a recurrence formula for the coefficients of the wave function of a quantum walker on an undirected graph with a finite number of nodes. By extending this formula to include extra layers, we develop a simulation model to describe the time evolution of the quantum walker on a multilayer network. The time-averaged probability and the return probability of the quantum walker are studied with Fourier, and Grover walks on multilayer networks. Furthermore, we analyze the impact of decoherence on quantum transport, shedding light on how environmental interactions may impact the behavior of quantum walkers on multilayer network structures.

Keywords: discrete-time quantum walks; multilayer network; decoherence

1. Introduction

Quantum walks (QWs) are the quantum analogs of classical random walks (CRWs). Importantly, QWs contribute to the theoretical and applied studies of quantum computing [1] and quantum algorithms [2]. There are two broad classes of QWs known as discrete-time QWs (DTQW) and continuous-time QWs (CTQW), each of which has significant distinctions in their mathematical formalism [3]. A considerable body of work can be found in the literature which explores the dynamics of linear and cyclic QWs in two and higher-dimensional spaces, as well as on specific graphs [3,4].

In the study of complex systems, multilayer networks play a crucial role as a modeling tool [5–7]. A multilayer network consists of nodes and edges, yet the edges exist in separate layers representing different forms of interactions. Multilayer networks are used to understand the evolution of ecological systems [8], complex interactions across multiple layers of biological systems [9], public transportation systems [10] and the structure of financial markets [11]. One can find several studies that utilize the framework of CTQWs to investigate transport properties of multilayer dendrimer networks [12], honeycomb networks [13], and important models of scale-free networks [14]. Nonetheless, it is clear that there has been insufficient exploration of the dynamics of DTQWs on multilayer networks. Therefore, we present a comprehensive study of DTQWs on a multilayer network to address this gap. Several formulations of the DTQWs on specific network structures can be found in the literature. However, defining a DTQWs on an arbitrary network is more difficult than that of a CTQWs [15]. Ref. [16] has proposed a framework for defining QWs on regular graphs. Sometimes, this framework is termed the Shunt-Decomposition model [17]. In [2], it is suggested to add one or more self-loops to each vertex with the purpose of obtaining a regular graph when modeling the QWs on irregular graphs. Redefining the action of the conditional swap operator in [18], Kendon [19] has presented a method to simulate DTQWs on general undirected graphs. Sometimes, this method is identified as



Citation: Jayakody, M.N.; Pradhan, P.; Ben Porath, D.; Cohen, E. Discrete-Time Quantum Walk on Multilayer Networks. *Entropy* **2023**, *25*, 1610. <https://doi.org/10.3390/e25121610>

Academic Editor: Rosario Lo Franco

Received: 29 September 2023

Revised: 24 November 2023

Accepted: 27 November 2023

Published: 30 November 2023



Copyright: © 2023 by the authors. Licensee MDPI, Basel, Switzerland. This article is an open access article distributed under the terms and conditions of the Creative Commons Attribution (CC BY) license (<https://creativecommons.org/licenses/by/4.0/>).

the arc-reversal model [17]. Ref. [20] has proposed another framework for QWs on a graph in which the motion of the quantum walker takes place on the edges of the graph rather than the vertices.

In our work, we give a block matrix representation for the state of the quantum walker instead of the usual column vector representation. Then, we derive formulae that imitate the coin toss and the shifting operation of the DTQW. Using these formulae and the block matrix representation, we develop a simulation to mimic the progression of DTQWs on an undirected graph. Later, we extend our framework to mimic DTQWs on multilayer networks.

The paper is organized in the following way. In Section 2, we present our mathematical model for DTQWs on a graph. Section 3 is dedicated to extending our mathematical model to include DTQWs on multilayer networks. Moreover, for comparison purposes, we also model a CRW on a multilayer network in Section 4. Numerical implementation of DTQWs on a toy model and some synthetic multilayer networks are given in Sections 5 and 6, respectively, along with a detailed analysis of time-average probability, return probability, and decoherence.

2. QWs on a Graph

Consider a finite undirected graph $\mathcal{G} = \{V, E\}$ where $V = \{v_1, \dots, v_n\}$ is the set of vertices (nodes) and $E = \{(v_i, v_j) \mid v_i, v_j \in V\}$ is the set of edges (connections). Note that, the graphs we studied here are finite as opposed to the unrestricted line or the integer line we used to define the QWs on a line [21]. Moreover, our study considers only simple graphs (i.e., graphs without self-loops or parallel edges). We denote the adjacency matrix corresponding to \mathcal{G} as $\mathbf{A} \in \mathbb{R}^{n \times n}$ which is defined in the following way

$$a_{ij} = \begin{cases} 1 & \text{If } (v_i, v_j) \in E \\ 0 & \text{Otherwise} \end{cases} \quad (1)$$

The positive integers $n = |V|$ and $m = |E|$ represent the number of nodes and edges in \mathcal{G} , respectively. The number of edges linked to a particular node v_i is referred to as its degree and denoted by $d_i = \sum_{j=1}^n a_{ij}$.

Let us now model the propagation of a QW on \mathcal{G} . For convenience, let us relabel the vertices of \mathcal{G} or, in the QWs' terminology, the position states of the QW as $|x\rangle_p$ where $x = 1, \dots, n$. Then, the set of vertices $V = \{|1\rangle_p, |2\rangle_p, \dots, |n\rangle_p\}$ becomes the position basis set of the QW which spans the position of the Hilbert space H_p . Let us denote the subspace spanned by the basis element $|x\rangle_p$ in V as $H_p^{(x)}$. That is, $H_p^{(x)} = \text{span}\{|x\rangle_p\}$ where $|x\rangle_p \in V$. Now, for each vertex $|x\rangle_p$, let us assign a coin Hilbert space $H_c^{(x)}$ spanned by the coin basis $\{|r\rangle_c \mid r = 1, \dots, d_x\}$ where d_x is the degree of the vertex $|x\rangle_p$. Note that, the dimension of the coin Hilbert space $H_c^{(x)}$ is d_x . To gain an advantage in simulation, we adopt the following strategy to modify the labeling of the coin states. We define a set \mathcal{B}_x that comprises the labels of the vertices adjacent to the vertex $|x\rangle_p$ as $\mathcal{B}_x = \{y : \text{vertex } |x\rangle_p \text{ and } |y\rangle_p \text{ have a connection}\}$ where $|\mathcal{B}_x| = d_x$. Now, we define a function as, $f_x(r) = r$ th element of \mathcal{B}_x . Since the parallel edges are excluded in our study, the function $f_x(r)$ is a bijection. Without the loss of generality, we always arrange the elements of \mathcal{B}_x in an ascending order. Now, we can denote the basis of the coin Hilbert space $H_c^{(x)}$ as $\{|f_x(r)\rangle_c \mid r = 1, \dots, d_x\}$. Using $f_x(r)$, we have labeled the coin states of each vertex in terms of the edges connected to it. Such an approach can be found in [18]. Now, the state vector of the quantum walker at position $|x\rangle_p$ at time t can be written as

$$|\psi(x, t)\rangle = \sum_{r=1}^{d_x} \alpha_{x, f_x(r)}(t) |x\rangle_p |f_x(r)\rangle_c \quad (2)$$

where $\alpha_{x,f_x(r)}(t) \in \mathbb{C}$ are called the probability amplitudes, $|x\rangle_p \in H_p^{(x)}$, $|f_x(r)\rangle_c \in H_c^{(x)}$ and $|\psi(x,t)\rangle \in H_p^{(x)} \otimes H_c^{(x)}$. Here, $\dim(H_p^{(x)}) = 1$, $\dim(H_c^{(x)}) = d_x$ and $\dim(H_p^{(x)} \otimes H_c^{(x)}) = d_x$. For each position x , the coefficient $\alpha_{x,r}(t) = 0$ whenever $r \notin \mathcal{B}_x$. Our next task is to write an expression for the total wave function of the quantum walker on \mathcal{G} at time t . For that, we need to sum the state vectors $|\psi(x,t)\rangle$ in (2) over all the vertices. However, we cannot perform such a summation because the state vectors $|\psi(x,t)\rangle$, corresponding to each vertex, reside in different composite Hilbert spaces as the size of $H_c^{(x)}$ changes with the degree of the node x . Therefore, to perform such a summation, one needs to combine the set of composite Hilbert spaces $\{H_p^{(x)} \otimes H_c^{(x)}\}_x$ in a reasonable manner to form a bigger Hilbert space that includes all the state vectors. The operation of the direct sum of the vector spaces paves a way to combine the composite Hilbert spaces to cater to our demand. Let us define $H = \bigoplus_{x=1}^n (H_p^{(x)} \otimes H_c^{(x)})$ where \oplus denotes the external direct sum of Hilbert spaces and $\dim(H) = \sum_{x=1}^n d_x$. According to the definition of the global Hilbert space H , it is obvious that for each vertex x , the state vector $|\psi(x,t)\rangle \in H$. Hence, the total wave function of the quantum walker at time t can be calculated by summing $|\psi(x,t)\rangle$ in (2) over all the vertices. Then, the total wave function at time t can be written as

$$|\psi_t\rangle = \sum_{x=1}^n \sum_{r=1}^{d_x} \alpha_{x,f_x(r)}(t) |x\rangle_p |f_x(r)\rangle_c \quad (3)$$

where $|\psi_t\rangle \in H$ and $\sum_{x=1}^n \sum_{r=1}^{d_x} |\alpha_{x,f_x(r)}(t)|^2 = 1$. Coin operator $C^{(x)}$, which acts on the coin states associated with the vertex $|x\rangle_p$, holds the transition probabilities from $|x\rangle_p$ to its neighboring vertices. Hence, $C^{(x)}$ can be defined as

$$C^{(x)} = \sum_{i=1}^{d_x} \sum_{j=1}^{d_x} C_{ij}^{(x)} |f_x(i)\rangle \langle f_x(j)| \quad (4)$$

where $\{|f_x(r)\rangle_c\}_{r=1}^{d_x}$ are the basis elements of $H_c^{(x)}$. The coin coefficients $C_{ij}^{(x)} \in \mathbb{C}$ are chosen in such a way that the condition of unitarity of the QW is preserved, i.e., the total probability is unity at all time steps. Hence, $(C^{(x)})^\dagger C^{(x)} = C^{(x)} (C^{(x)})^\dagger = \mathbb{I}$. By combining each local coin operator $C^{(x)}$, one can write the global coin operator C acting on $|\psi_t\rangle \in H$ as follows

$$C = \sum_{x=1}^n \sum_{i=1}^{d_x} \sum_{j=1}^{d_x} C_{ij}^{(x)} |x\rangle \langle x| \otimes |f_x(i)\rangle \langle f_x(j)| \quad (5)$$

The shift operator of the QW on a graph is defined as follows

$$S|x\rangle_p |y\rangle_c = |y\rangle_p |x\rangle_c \quad (6)$$

Note that the abstract forms of C and S given in (5) and (6), respectively, are similar to those used in the arc-reversal model [17]. However, the arc-reversal model and our method significantly differ in numerical simulation (discussed in Appendix A). Both C and S are unitary operators associated with the Hilbert space H . Hence, a single-step progression of the quantum walker on the graph is given by

$$|\psi_{t+1}\rangle = U|\psi_t\rangle \quad (7)$$

where $U = SC$ is the evolution operator and S and C are the shift and coin operators, respectively.

2.1. Matrix Representation and Simulation

The local coin operator $C^{(x)}$, associated with the vertex $|x\rangle_p$, holds the transition probabilities from $|x\rangle_p$ to its neighboring nodes. Suppose that the vertex $|x\rangle_p$ is linked to a d_x number of vertices denoted by $|y_1\rangle_p, \dots, |y_{d_x}\rangle_p$ and $y_1 < y_2 < \dots < y_{d_x}$. Hence, for each $r \in \{1, \dots, d_x\}$, we can write $y_r = f_x(r)$. Then, the block matrix of $C^{(x)}$ can be written as

$$C^{(x)} = \begin{pmatrix} \langle f_x(1)| & \dots & \langle f_x(d_x)| \\ |f_x(1)\rangle & C_{11}^{(x)} & \dots & C_{1d_x}^{(x)} \\ \vdots & \vdots & \ddots & \vdots \\ |f_x(d_x)\rangle & C_{d_x1}^{(x)} & \dots & C_{d_xd_x}^{(x)} \end{pmatrix} \quad (8)$$

For example, the local coin operators associated with a four-vertex graph are shown in Appendix A. In the standard mathematical formalism of QWs [21], a column vector represents the state of the quantum walker at time t . However, alternatively, one can give a convenient block matrix representation for the total wave function of the quantum walker on a graph given in (3) as follows

$$|\psi_t\rangle = \mathbf{N}_t = \begin{pmatrix} |1\rangle_c & \dots & |n\rangle_c \\ |1\rangle_p & \alpha_{1,1}(t) & \dots & \alpha_{1,n}(t) \\ \vdots & \vdots & \ddots & \vdots \\ |n\rangle_p & \alpha_{n,1}(t) & \dots & \alpha_{n,n}(t) \end{pmatrix} \quad (9)$$

In matrix \mathbf{N}_t , the rows represent the position states, and the columns represent the coin states. A single row holds the coefficients corresponding to the coin states associated with a single position. According to the definition of the coefficients of $\alpha_{x,r}(t)$, some entries of the matrix \mathbf{N}_t become zero (Appendix A). Such a block matrix representation of the total wave function can be found in the study [22]. One can view the block matrix representation given in (9) as an adjacency matrix of a weighted graph with time-dependent complex weights. By knowing all the coefficients of $\alpha_{x,r}(t)$, in other words, all the elements of \mathbf{N}_t , we can uniquely determine the total wave function of the quantum walker on the graph at time t . In addition, by appropriately updating the elements of \mathbf{N}_t , one can determine the matrix \mathbf{N}_{t+1} and hence the total wave function of the quantum walker at time $t + 1$. The elements of \mathbf{N}_t are updated in two processes. First, an intermediate matrix $\tilde{\mathbf{N}}_t$ is generated using the following formula

$$\tilde{\alpha}_{x,f_x(i)}(t) = \sum_{j=1}^{d_x} \alpha_{x,f_x(j)}(t) C_{ij}^{(x)} \quad (10)$$

Afterwards, the matrix \mathbf{N}_{t+1} is determined by taking the transpose of $\tilde{\mathbf{N}}_t$. The update rule is given by

$$\alpha_{x,f_x(i)}(t+1) = \tilde{\alpha}_{f_x(i),x}(t) \quad (11)$$

Note that the expression in (10) and the recurrence formula in (11) correspond to the coin and shift operations of the QW on the graph, respectively. The proof is given in the Appendix B.

2.2. Probability Calculation

The probability $P_q(x, t)$ of finding the quantum walker at vertex x at time t can be calculated using (2) as follows

$$P_q(x, t) = \sum_{r=1}^{d_x} |\alpha_{x,f_x(r)}(t)|^2 \quad (12)$$

Note that $P_q(x, t)$ can be determined by summing the elements in the x th row of the matrix $\mathbf{N}_t \odot \mathbf{N}_t^*$ where \odot is the Hadamard product of matrices and \mathbf{N}_t^* is the complex conjugate of the block matrix given in (9).

3. QWs on Multilayer Networks

A multilayer network is a pair $\mathcal{M} = (\mathcal{G}, \mathcal{C})$ where $\mathcal{G} = \{\mathcal{L}_\alpha; \alpha \in \{1, 2, \dots, l\}\}$ is a family of undirected graphs of $\mathcal{L}_\alpha = \{V_\alpha, E_\alpha\}$ (called layers of \mathcal{M}) with $V_\alpha = \{v_1^\alpha, v_2^\alpha, \dots, v_{n_\alpha}^\alpha\}$ is the set of vertices and $E_\alpha = \{e_1^\alpha, e_2^\alpha, \dots, e_{r_\alpha}^\alpha : e_{r_\alpha} = (v_i^\alpha, v_j^\alpha)\}$ is the set of edges in the \mathcal{L}_α layer of the multilayer network [6]. The positive integers l , n_α and r_α are termed as the number of layers in \mathcal{M} , the number of vertices and the edges of the layer \mathcal{L}_α respectively. Moreover, $\mathcal{C} = \{E_{\alpha\beta} \subseteq V_\alpha \times V_\beta : \alpha, \beta \in \{1, 2, \dots, l\}, \alpha \neq \beta\}$ is the set of edges between the \mathcal{L}_α and \mathcal{L}_β layers. The elements of \mathcal{C} are crossed layers. Furthermore, the elements of each E_α are called the set of intralayer edges, and the elements of each $E_{\alpha\beta}$ ($\alpha \neq \beta$) are called the interlayer edges of \mathcal{M} [23]. Let us denote the adjacency matrices corresponding to each layer \mathcal{L}_α as $A^{(\alpha)} = (a_{ij}^\alpha) \in \mathbb{R}^{n_\alpha \times n_\alpha}$ which is defined by

$$a_{ij}^\alpha = \begin{cases} 1 & \text{If } (v_i^\alpha, v_j^\alpha) \in E_\alpha \\ 0 & \text{Otherwise} \end{cases} \quad (13)$$

for $1 \leq i, j \leq n_\alpha$ and $1 \leq \alpha \leq l$ where n_α is the number of nodes in layer \mathcal{L}_α . The interlayer adjacency matrix corresponding to $E_{\alpha\beta}$ is the matrix $A^{[\alpha, \beta]} \in \mathbb{R}^{n_\alpha \times n_\beta}$ given by

$$a_{ij}^{\alpha\beta} = \begin{cases} 1 & \text{If } (v_i^\alpha, v_j^\beta) \in E_{\alpha\beta} \\ 0 & \text{Otherwise} \end{cases} \quad (14)$$

By appropriately combining the adjacency matrices corresponding to each layer \mathcal{L}_α and the interlayer adjacency matrices, one can derive a supra-adjacency matrix [23] which characterizes \mathcal{M} . Now, let us define a QW on \mathcal{M} . Recall that, in Section 2, we developed a mathematical model to mimic the propagation of a QW on any given undirected graph. According to our model, when the adjacency matrix is given, we define the sets of $\{\mathcal{B}_x\}_{x=1}^n$ along with the set of functions $\{f_x(r)\}_{x=1}^n$ and then simulate the evolution of the QW on the graph by updating the elements of the block matrix in (9). Likewise, one can use the same mathematical model to mimic the propagation of a quantum walker on a multilayer network just by following the same procedure given in Section 2 with the supra-adjacency matrix of \mathcal{M} . In a QW, the transition probabilities from vertex x to its neighboring vertices are given by the coin operator $C^{(x)}$. According to the simulation, one can choose suitable coin operators to control the probability flow from one vertex to the neighboring vertices in the multilayer network. When the transition probabilities from a vertex x to its neighboring vertices are the same, we say that the QW on the multilayer network is unbiased. To model such an unbiased QW, we can attach a Fourier coin $F^{(x)}$ to each vertex x given by

$$F^{(x)} = \frac{1}{\sqrt{d_x}} \sum_{r=1}^{d_x} \sum_{s=1}^{d_x} e^{2i\pi(r-1)(s-1)/d_x} |r\rangle \langle s| \quad (15)$$

where d_x is the degree of vertex x [24]. Note that, the relationship of $F^{(x)}(F^{(x)})^\dagger = (F^{(x)})^\dagger F^{(x)} = \mathbb{I}$ is preserved by the Fourier coin. In the studies of QWs on graphs, it has been shown that the Grover coin tends to localize the quantum walker around the initial vertex [24]. Hence, it is also worth exploring the Grover's walk on a multilayer network. The ij th element of the Grover coin $G^{(x)}$ attached to the vertex x on \mathcal{M} can be written as

$$G_{ij}^{(x)} = \begin{cases} \frac{2-d_x}{d_x} & \text{If } i = j \\ \frac{2}{d_x} & \text{Otherwise} \end{cases} \quad (16)$$

where $1 \leq i, j \leq d_x$ and d_x is the degree of vertex x . Note that, the Grover coin holds the relationship of $G^{(x)}(G^{(x)})^\dagger = (G^{(x)})^\dagger G^{(x)} = \mathbb{I}$. In Sections 5 and 6, we analyze the dynamics of some QWs on specific multilayer networks with different choices of coin operators. Note that a multilayer network can be conceptualized as a single-layer network with different groups of nodes, each having distinct connection properties. Hence, the general definition of discrete-time QWs on the undirected graph in Section 2 already captures the case of QWs on multilayer networks. However, since the multilayer networks offer a more detailed and comprehensive representation of complex systems [25], the framework for QWs on multilayer networks, which we have given in this paper, can be conveniently used to model and analyze complex scenarios. For instance, our framework for QWs on multilayer networks enables the modeling and analyzing of the situation in which each layer possesses a different coin (Appendix C and Figure A2).

4. Classical Random Walk on Multilayer Networks

The propagation of the classical random walk (CRW) on different graph structures is a topic that has been extensively studied [26]. In general, the propagation of a random walker on any given network structure is modeled using the transition probabilities from a vertex x to its neighboring vertices [19,27]. By adopting the same concept, one can also define a CRW on a multilayer network [28]. Let $\Omega_{x,y}$ be the transition probability from vertex x to y . Then, the probability $P_c(x, t)$ of finding the random walker at position x at time t is given by the following recurrence relations

$$P_c(x, t) = \sum_{r=1}^{d_x} \Omega_{f_x(r), x} P_c(f_x(r), t-1) \quad (17)$$

where d_x is the degree of the vertex x and for each r , the function $f_x(r)$ gives the labels of the neighbouring vertices of x . When the transition probabilities from a vertex x to its neighboring vertices are the same, we say the CRW is unbiased. In usual practice [27], transition probability $\Omega_{x,y}^{(ub)}$ for the unbiased classical random walk (UBCRW) on any graph structure is defined as follows

$$\Omega_{x,y}^{(ub)} = \begin{cases} \frac{1}{d_x} & \text{If } (x, y) \text{ is connected} \\ 0 & \text{Otherwise} \end{cases} \quad (18)$$

where d_x is the degree of vertex x . One can adopt the same definition given in (18) to model the UBCRW on a multilayer network.

5. Numerical Implementation on a Toy Model

In this section, we perform the UBCRW and the Fourier walk (unbiased QW) on a toy multilayer network structure (Figure 1) and examine the flow of probability through various layers. We intend to explore the fundamental differences between classical and quantum dynamics on a multilayer network. From the definition of the multilayer network given in Section 3, one can consider diverse configurations of structures with multilayers. Nonetheless, a two-layer network consisting of two distinct graphs can be understood as the simplest multilayer network. Hence, we consider one such simplest multilayer structure to perform the UBCRW and the Fourier walk. Note that the interlayer edges of the toy model in Figure 1 only link the vertices representing the same entity in different layers. Hence, this network can be classified as a multiplex network, which is a special class of multilayer networks [29]. Let the top and bottom layers be $\mathcal{L}_1 = \{V_1, E_1\}$ and $\mathcal{L}_2 = \{V_2, E_2\}$ respectively where $V_1 = \{1, 2, 3, 4\}$ and $V_2 = \{5, 6, 7, 8\}$ are the set of vertices in each layer and E_1 and E_2 are the set of edges corresponding to each layer. The supra-adjacency matrix [23] of the multilayer network in Figure 1 can be written as follows

$$A_{sup} = \left(\begin{array}{c|c} A^{(1)} & \mathbb{I} \\ \hline \mathbb{I} & A^{(2)} \end{array} \right) = \left(\begin{array}{cccc|cccc} 0 & 1 & 1 & 1 & 1 & 0 & 0 & 0 \\ 1 & 0 & 1 & 1 & 0 & 1 & 0 & 0 \\ 1 & 1 & 0 & 1 & 0 & 0 & 1 & 0 \\ 1 & 1 & 1 & 0 & 0 & 0 & 0 & 1 \\ \hline 1 & 0 & 0 & 0 & 0 & 1 & 0 & 1 \\ 0 & 1 & 0 & 0 & 1 & 0 & 1 & 0 \\ 0 & 0 & 1 & 0 & 0 & 1 & 0 & 1 \\ 0 & 0 & 0 & 1 & 1 & 0 & 1 & 0 \end{array} \right) \quad (19)$$

where the first ($A^{(1)}$) and second ($A^{(2)}$) block matrices along the diagonal (i.e., the top-left corner and bottom-right corner) represent the adjacency matrices of the layer \mathcal{L}_1 and \mathcal{L}_2 respectively. The top-right and bottom left block matrices represent the connection between the layers. Using the supra-adjacency matrix in (19), one can define the sets of $\{\mathcal{B}_x\}_{x=1}^8$ along with the set of functions $\{f_x(r)\}_{x=1}^8$ and then simulate the evolution of the QW on the multilayer network by updating the elements of the block matrix in (9).

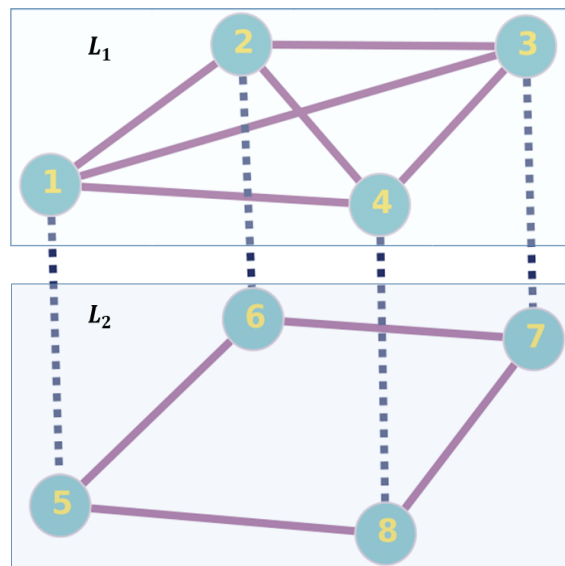


Figure 1. A multilayer network with four vertices and two layers named L_1 and L_2 . The set of labels $\{x, x + 4\}$ where $x \in \{1, 2, 3, 4\}$ represent the same entity in different layers. The solid lines connect the vertices within each layer, and the dotted lines connect interlayer. The top layer represents an undirected regular graph, and the bottom layer represents an undirected connected graph. This schematic diagram is inspired by [6,7].

5.1. Probability Distribution

We perform the UBCRW and the Fourier walk on the toy multilayer network structure and investigate the probability of finding the walker on each layer after 100 steps. The UBCRW is initialized from the vertex 1, and the Fourier walk is initialized from two localized initial states of the form $|1\rangle_p \otimes |3\rangle_c$ and $|1\rangle_p \otimes |5\rangle_c$. We place the quantum walker at the position state $|1\rangle_p$ (vertex 1), attaching the coin state of $|3\rangle_c$ and $|5\rangle_c$ to the walker. We select these localized initial states to replicate the conditions similar to those in the UBCRW, which enables a meaningful comparison between the unbiased CRW and QW on the toy multilayer model. After 100 steps, we calculate the probability of finding the walker at each layer by summing the probability of finding the walker at each node corresponding to a given layer. An interesting distinction between the unbiased classical and quantum walkers is illustrated in Figure 2. For the case of UBCRW, the probabilities of finding the walker on the top and bottom layers eventually stabilize to a steady state as time progresses (Figure 2a). Conversely, the Fourier walk displays dynamic changes in probability over time (Figure 2b,c).

It is important to note that, in the case of UBCRW, the probability of locating the walker on the top layer is consistently higher than that of the bottom layer, which is expected since the top layer comprises a complete graph. However, in the Fourier walk, certain time steps exist where the probability of locating the walker on the bottom layer surpasses that of the top layer. For instance, in Figure 2c, one can see certain time steps where the probability of finding the walker on the bottom layer is higher than that of the top layer. In addition, from Figure 2b,c, one can identify that the different initial coin states of the Fourier walk can control the temporary transition of the quantum walker from top layer to bottom layer. Such a behavior has no analogy to the UBCRW. The ability of the Fourier walker to temporarily transit from the top layer to the bottom, with higher probability, implies that the Fourier walk could explore a broader portion of the multilayer structure compared to the UBCRW. This enhanced exploration could be useful when searching through large, complex databases represented as multilayer networks. In Section 6, we further examine this behavior by employing different types of larger multilayer networks.

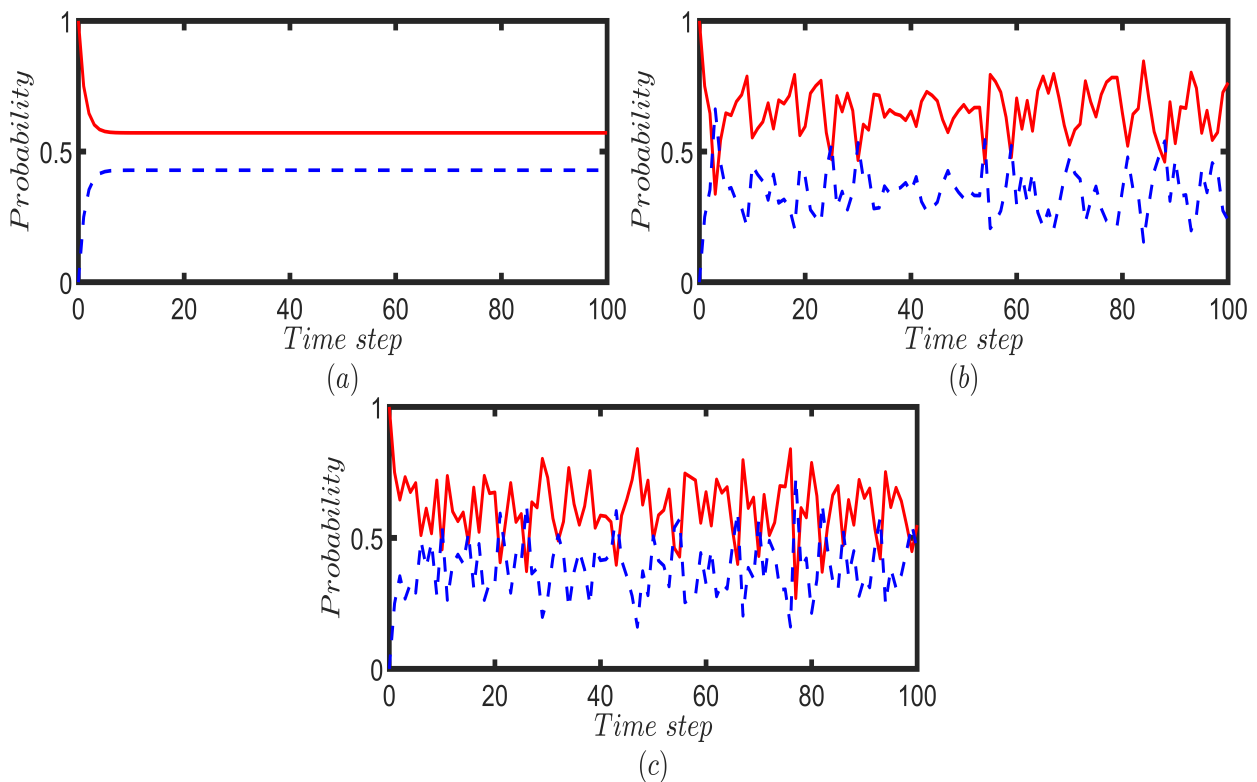


Figure 2. Probability of finding the walker on the top layer (red solid line) and bottom layer (blue dotted line) for each time step up to 100 steps **(a)** unbiased CRW is initiated from vertex 1. Fourier walk is initiated from **(b)** $|1\rangle_p \otimes |3\rangle_c$ and **(c)** $|1\rangle_p \otimes |5\rangle_c$.

In Figure 2b,c, we have seen that the quantum probability is fluctuating. This behavior is attributed to the unitary characteristic of QWs, which prevents the quantum walker from reaching a steady state [30]. Hence, to obtain an idea of the static picture, one can calculate the time-averaged probability of finding the quantum walker at vertex x defined by

$$\bar{P}_T(x) = \frac{1}{T} \sum_{t=0}^{T-1} P_q(x, t) \quad (20)$$

where $T \in \mathbb{N}$ [3]. Note that when T becomes larger, $\bar{P}_T(x)$ becomes a better measure that depicts the static picture. In Figure 3, we illustrate the time-averaged probabilities for a time period of $T = 100$ for Fourier and Grover walks on the toy network model. For the sake of comparison, we calculate the probability profile of the UBCRW as well (Figure 3a).

The vertical axis of the heatmaps in Figure 3 represents the initial node from which the walker starts the walk, while the horizontal axis represents the target node where the walker ends the walk. For both Fourier and Grover walk, we consider two cases. In the first case, we initiate both Fourier and Grover walkers from the localized initial state of the form $|\phi_1\rangle \equiv |x\rangle_p \otimes \frac{1}{\sqrt{d_x}} \sum_{r=1}^{d_x} |f_x(r)\rangle_c$ where $x \in \{1, \dots, 8\}$. We start both QWs from each node by attaching a uniform superposition of coin states. Then, for each node, the time-averaged probability for a time period of $T = 100$ is calculated using (20). The results are given in Figure 3b,c. In the second case, we repeat the same procedure by using the localized initial state of the form $|\phi_2\rangle \equiv |x\rangle_p \otimes \left(\frac{i}{\sqrt{d_x}} |f_x(1)\rangle_c + \frac{1}{\sqrt{d_x}} \sum_{r=2}^{d_x-1} |f_x(r)\rangle_c - \frac{i}{\sqrt{d_x}} |f_x(d_x)\rangle_c \right)$ where $x \in \{1, \dots, 8\}$. The results are given in Figure 3d,e. According to Figure 3a, the classical walker tends to stay on the top layer of the toy model after 100 time steps, irrespective of its initial node. Since the top layer comprises a complete graph, we can expect this result. The time-average probability profile of the Fourier walk also exhibits similar behavior to the classical walker when initiated from $|\phi_1\rangle$. That is, the time-average probability of finding the Fourier walker on the top layer is relatively higher than that of the bottom layer, irrespective of the initial node.

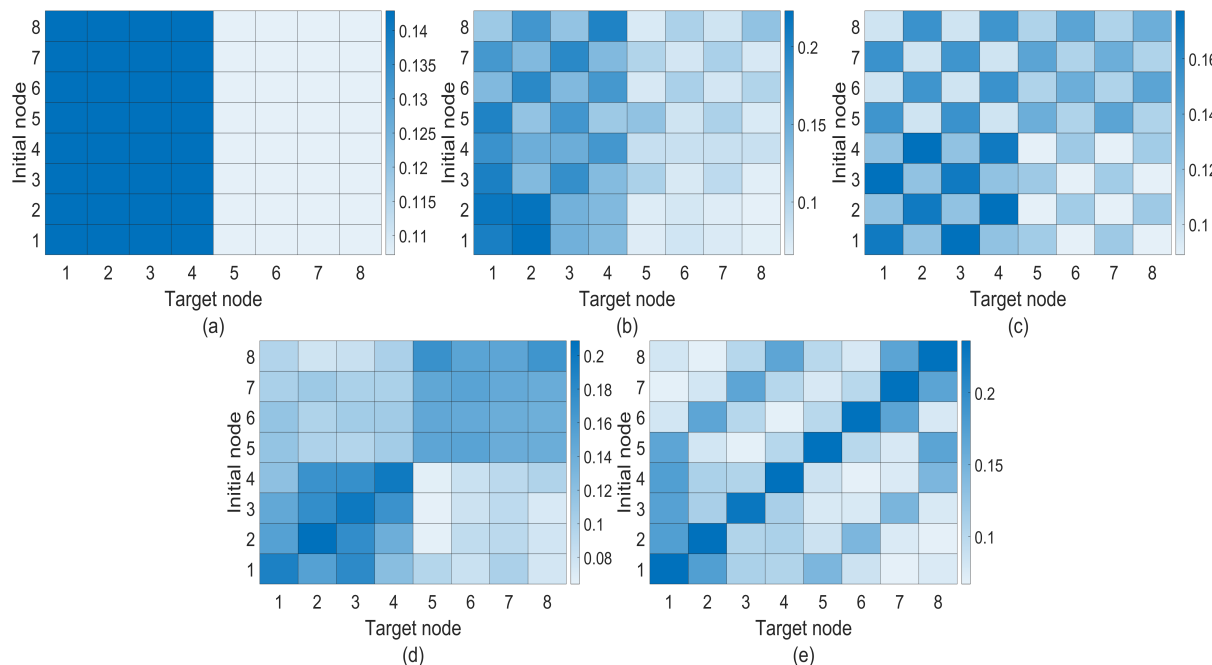


Figure 3. Heatmaps are depicted for (a) unbiased CRW, (b,d) Fourier walk, and (c,e) Grover walk. The vertical axis shows the initial node from which the walker starts the walk, and the horizontal axis shows the target node where the walker ends the walk. Each square corresponding to the Fourier and Grover walks indicates the value of time-averaged probabilities for a time period of $T = 100$. For the unbiased CRW, each square corresponds to the probability after 100 time steps. Both Fourier and Grover walks in (b,c) are initiated from the localized position state $|\phi_1\rangle \equiv |x\rangle_p \otimes \frac{1}{\sqrt{d_x}} \sum_{r=1}^{d_x} |f_x(r)\rangle_c$ and for (d,e) walks are initiated from the localized position state $|\phi_2\rangle \equiv |x\rangle_p \otimes \left(\frac{i}{\sqrt{d_x}} |f_x(1)\rangle_c + \frac{1}{\sqrt{d_x}} \sum_{r=2}^{d_x-1} |f_x(r)\rangle_c - \frac{i}{\sqrt{d_x}} |f_x(d_x)\rangle_c \right)$. Note that, $|\phi_1\rangle$ and $|\phi_2\rangle$ have a uniform superposition of coin states, yet $|\phi_2\rangle$ contains some complex coefficients.

However, when the Fourier walker is initiated from $|\phi_2\rangle$, we can confine the walk to a particular layer with a higher probability, which is visible in Figure 3d. When initiated from $|\phi_1\rangle$, Grover walk exhibits no significant behavior, but for the initial condition of $|\phi_2\rangle$, Grover walker tends to stay, with a higher probability, at the initial position and the corresponding position on the other layer. As a result, one can see a sharp line along the

diagonal of the grid in Figure 3e and two lines parallel to this sharp diagonal line. Hence, one can control the quantum dynamics on the multilayer network by changing the initial state, which has no direct analogy in UBCRW.

5.2. Return Probability

Another interesting question one could ask related to CRWs or QWs on a multilayer network is that of how long it would take for the walker to return to its initial position. This could be understood as the recurrence of the walk on the multilayer network. Recurrence in a CRW is characterized by the Pólya number [31], which can be written as

$$P = 1 - \frac{1}{\sum_{t=1}^{\infty} P(x_0, t)} \quad (21)$$

where $P(x_0, t)$ is the probability of finding the walker at the initial node x_0 at time step t . For $P = 1$, the walk is identified as *recurrent*. Otherwise, the walk is called *transient*. Moreover, the expression

$$P = 1 - \Pi_{t=1}^{\infty} [1 - P(x_0, t)] \quad (22)$$

can also be used as a definition for the Pólya number as it provides the same criteria for the classification of the walk [32]. With the formula given in (22), the notion of Pólya number can be extended to the study of recurrence in QWs [32,33]. For practical purposes, one can calculate the partial Pólya number using either (21) or (22) for a finite number of time steps $t = T_p$ rather than extending $t \rightarrow \infty$. We calculate the partial Pólya number for UBCRW as well as Grover and Fourier walks on the toy multilayer network by choosing a set of finite time steps $T_p \in \{0, 5, 10, \dots, 200\}$ with a gap of 5 units. Our purpose is to make an estimation of the convergence of the Pólya number for each walk. We initialize the walker from node 1, and for both Grover and Fourier walks, the initial coin state is chosen as the uniform superposition of coin states (i.e., $|1\rangle_p \otimes \frac{1}{\sqrt{d_1}} \sum_{r=1}^{d_1} |f_1(r)\rangle_c$). Figure 4 shows the convergence of the partial Pólya number for UBCRW, Grover, and Fourier walks. According to Figure 4, Grover and Fourier walkers exhibit recurrence during the progression of the walk on the toy multilayer structure. However, the Grover walker returns to its initial position faster than the Fourier and unbiased classical walker.

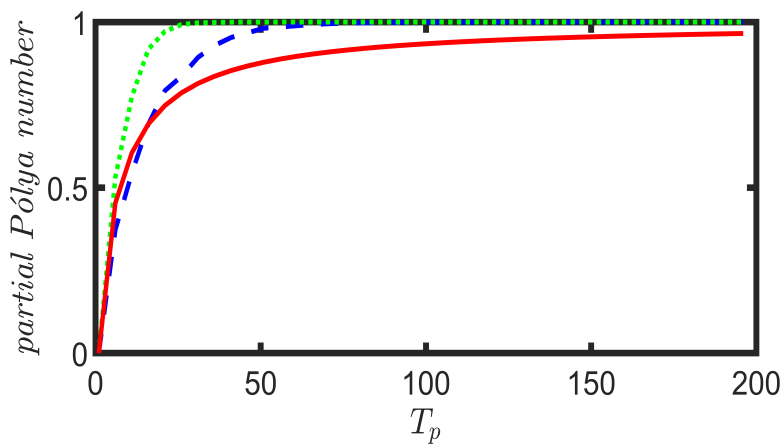


Figure 4. Convergence of the partial Pólya number for Grover (green dotted line), Fourier (blue dash line), and unbiased classical (red solid line) walkers on the toy multilayer network. The Partial Pólya number is calculated by choosing a set of finite time steps $T_p \in \{0, 5, 10, \dots, 200\}$ with a gap of 5 units. Each walk is initiated from node 1, and for both the Grover and Fourier walks, the initial coin state is chosen as the uniform superposition of coin states.

5.3. Impact of Decoherence

This section is devoted to study the impact of decoherence on the quantum dynamics of the walker that propagates on the toy multilayer network model. With regard to this, we study the impact of decoherence that arises from randomly broken links. In the context of QWs on graphs, broken link decoherence specifically relates to the loss of coherence in a QW due to imperfections or disruptions in the graph structure [34,35]. This can occur when edges in the graph are altered or removed, creating discontinuities in the QW. These disruptions can be caused by various factors, including physical imperfections, noise, or intentional modifications to the graph.

We perform a Fourier walk for 100 time steps on the toy multilayer network model while breaking the connection between nodes 1 and 3 with a 0.5 probability at each time step. Afterward, the mean probability distribution was calculated by averaging over 1000 trials. Figure 5c displays the mean probability distribution of the Fourier walk over 100 time steps when subjected to the broken link decoherence model. Additionally, for comparison purposes, the probability distributions of the UBCRW and the standard Fourier walk are also presented in Figures 5a and 5b, respectively. According to Figure 5a, the classical walker tends to stay on the top layer with higher probability after 100 time steps, a behavior which we have consistently seen in Figures 2 and 3. On the other hand, the standard Fourier walk exhibits a very different probability profile compared to the UBCRW, as shown in Figure 5b.

However, when subjected to a broken link decoherence model, the classical signature emerges in the average probability distribution of the Fourier walk as depicted in Figure 5c. Recall that, in this study, we have realized the broken link decoherence model by breaking the connection between nodes 1 and 3 of the toy multilayer network model with a 0.5 probability at each time step. That is, we allow to alter only a single edge in the toy multilayer network. Yet, the effect of decoherence substantially impacts the dynamics of the walk, eventually converging it to the classical distribution. This implies that QWs on a multilayer network could be sensitive to decoherence models like broken links.

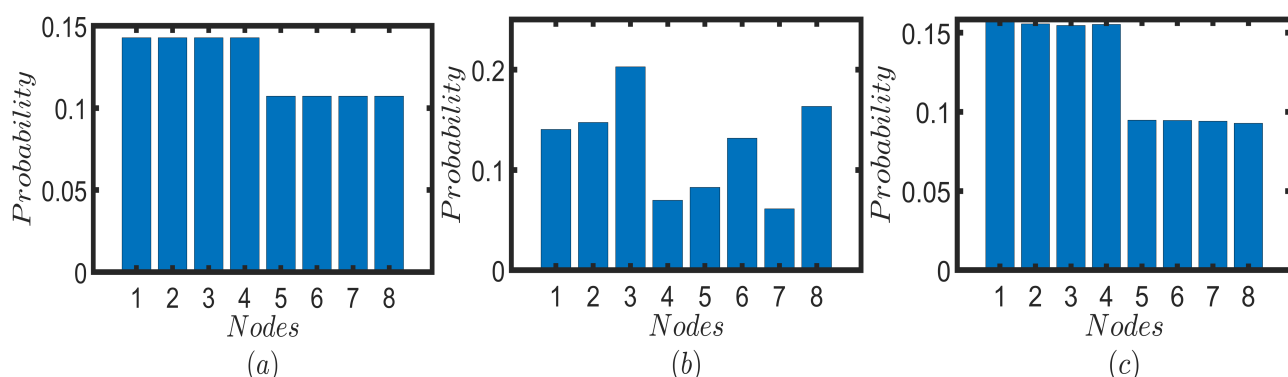


Figure 5. Probability distributions of the (a) unbiased CRW and (b) the standard Fourier walk after 100 time steps on the toy multilayer network. The unbiased CRW is initiated from node 1, and the Fourier walk is initiated from the localized state of $|1\rangle_p \otimes |2\rangle_c$. (c) The mean probability distribution of the Fourier walk subjected to the broken link decoherence model is generated by breaking the connection between nodes 1 and 3 of the toy multilayer network with a 0.5 probability at each time step and by averaging over 1000 trials.

6. Numerical Implementation on Synthetic Multilayer Networks

We next apply our model to perform QWs on six different two-layered multiplex networks, each consisting of 100 nodes. The top and bottom layers of each multiplex network are constructed from the combinations of scale-free (SF), complete (CP), and star networks with 50 nodes. Moreover, the walker is initiated from a randomly chosen node for the CP and SF networks and from the hub node in the case of the star network. First, we perform the Fourier walk on the two-layered multiplex networks, which is initiated from

the localized state of $|1\rangle_p \otimes \frac{1}{\sqrt{d_1}} \sum_{r=1}^{d_1} |f_1(r)\rangle_c$. For each time step, up to 100 time steps, we calculate the probability of finding the walker on each layer by summing the probabilities of finding the walker at each node corresponding to that layer (Figure 6). For comparison purposes, we perform the UBCRW on the same two-layered multiplex network structures (Figure A4). The unbiased classical walker is initiated from node 1.

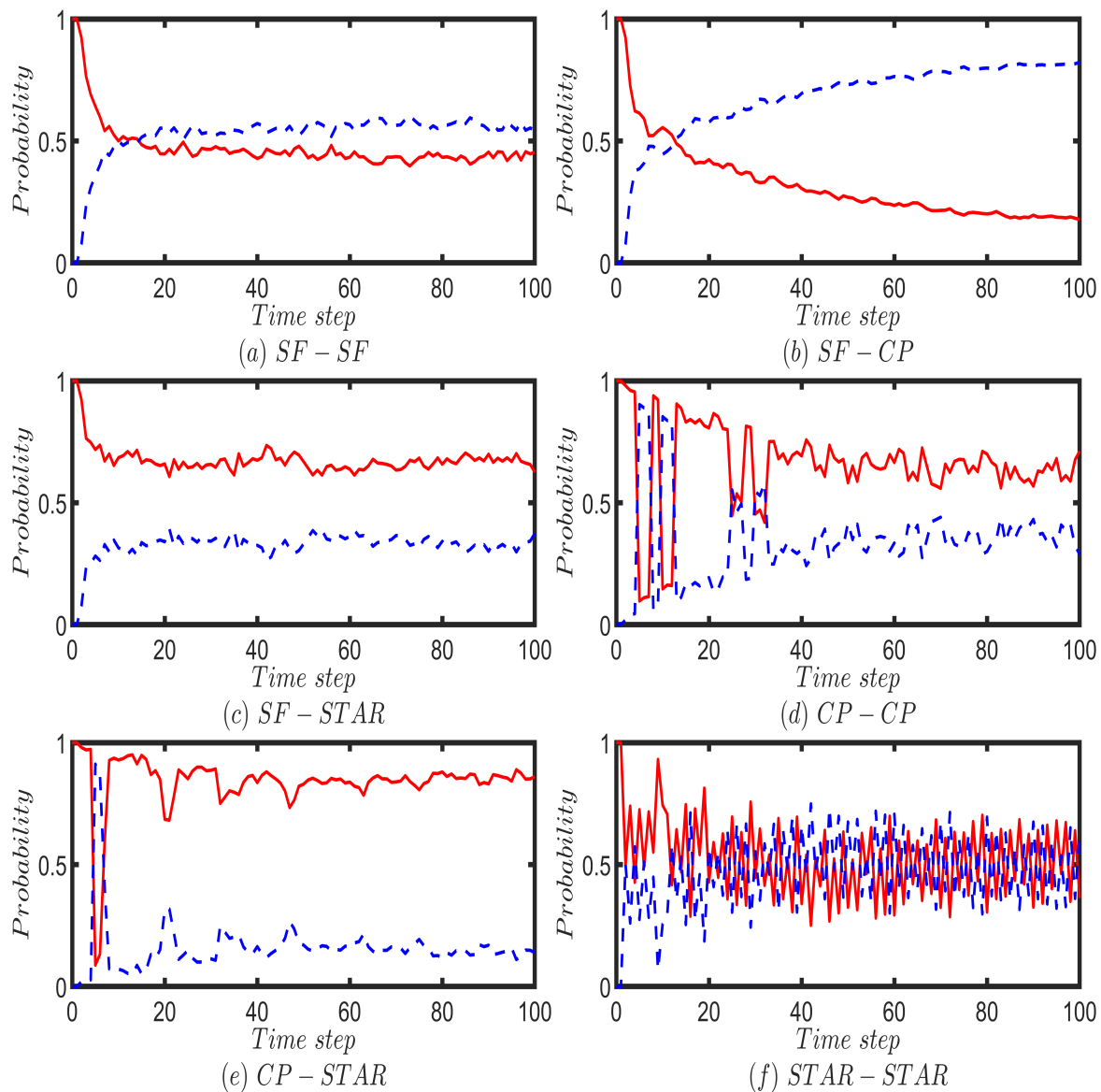


Figure 6. Illustrates the probability of finding the Fourier walker on the top layer (red solid line) and the bottom layer (blue dotted line) of six different two-layered multiplex networks, each consisting of 100 nodes. The top and bottom layers of each multiplex network are constructed from combinations of scale-free (SF), complete (CP), and star networks with 50 nodes. For the case of SF-SF, two different scale-free networks are chosen. Fourier walk is initiated from the localized position state of the form $|1\rangle_p \otimes \frac{1}{\sqrt{d_1}} \sum_{r=1}^{d_1} |f_1(r)\rangle_c$ and for each time step up to 100 steps, the probability of finding the walker on a given layer is calculated by summing the probabilities of finding the walker at each node corresponding to that layer.

By comparing the results in Figures 6 and A4, one can conclude that the probability of finding the Fourier and classical walkers on most of the multiplex networks follow a similar trend. However, for the cases of CP-CP, CP-STAR, and STAR-STAR, Fourier walk shows slight differences in its probability profiles in the first few time steps compared to the UBCRW (Figures 6d–f and A4d–f). Nonetheless, as time elapses, the overall trend of the probability profiles of the Fourier walker becomes similar to that of the UBCRW.

The probability profiles of the Grover walk on the six different multiplex networks are given in Figure 7. The Grover walker is also initiated from the localized state of $|1\rangle_p \otimes \frac{1}{\sqrt{d_1}} \sum_{r=1}^{d_1} |f_1(r)\rangle_c$ and for each time step up to 100 time steps, we calculate the probability of finding the walker on each layer by summing the probabilities of finding the walker at each node corresponding to that layer. On average, for the cases of SF-SF and SF-STAR, the Grover walker tends to be on both layers with an equal probability. This can be identified from Figure 7a,c. Grover walker on the CP-STAR multiplex network behaves in a very similar way to a classical walker (Figures 7e and A4e). A periodic behavior of the probability of finding the Grover walker on top and bottom layers can be seen on CP-CP and STAR-STAR multiplex networks (Figure 7d,f). The periodicity reflects Grover walker's coherent oscillations between the network layers and could be influenced by the topology and connectivity of the CP-CP and STAR-STAR multiplex network. Further research and analysis are essential to unlock the full potential of these insights for practical quantum applications.

In addition to exploring probability profiles, we have studied the recurrence probability of the Fourier, Grover, and unbiased classical walkers on the six different multiplex networks. We calculate the partial Pólya number for the UBCRW, Grover, and Fourier walks by choosing a set of finite time steps $T_p \in \{0, 5, 10, \dots, 100\}$ with a gap of 5 units. Our purpose is to make an estimation of the convergence of the Pólya number for each walk. We initialize each walker from node 1, and for both Grover and Fourier walks, the initial coin state is chosen as the uniform superposition of coin states (i.e., $|1\rangle_p \otimes \frac{1}{\sqrt{d_1}} \sum_{r=1}^{d_1} |f_1(r)\rangle_c$). Figure 8 shows the convergence of the partial Pólya number for the UBCRW, Grover, and Fourier walks. From Figure 8, one can identify that the Grover walk exhibits recurrence on most of the network structures. On the other hand, Fourier and unbiased classical walkers show no recurrence within 100 time steps. For all the plots in Figure 8, initially, the convergence of the partial Pólya number of the Fourier walk is low compared to that of the unbiased classical walker. However, as time elapses, the convergence of the Fourier walk surpasses that of the UBCRW, except for the case of the STAR-STAR multiplex network.

We apply the broken link decoherence model for the six different multiplex networks as well by following the same procedure described in Section 5. To realize the broken link decoherence model, we have removed some intralayer edges of the multiplex networks randomly and have calculated the average probability distribution of the QW after 100-time steps by averaging over 1000 trials. In Section 5, we observed the emergence of classical signature in the probability distribution even for a single broken link on the toy multilayer network. However, since the number of nodes in the six different multiplex networks is relatively large, we could not observe a fast convergence to the classical behavior when a single edge is broken. Nonetheless, when the number of broken links increases, the convergence to the classical distribution seems to be faster (Figure A3). This appears to imply that the impact of decoherence depends on the number of broken edges—a claim that should be further quantified and generalized in future research. While our investigation has shed some light on decoherence in multilayer networks, it is important to acknowledge that the scope of this research is not fully comprehensive. There remains significant potential for future studies to expand upon these findings to gain a deeper understanding of how decoherence impacts the propagation of the quantum walker on multilayer networks.

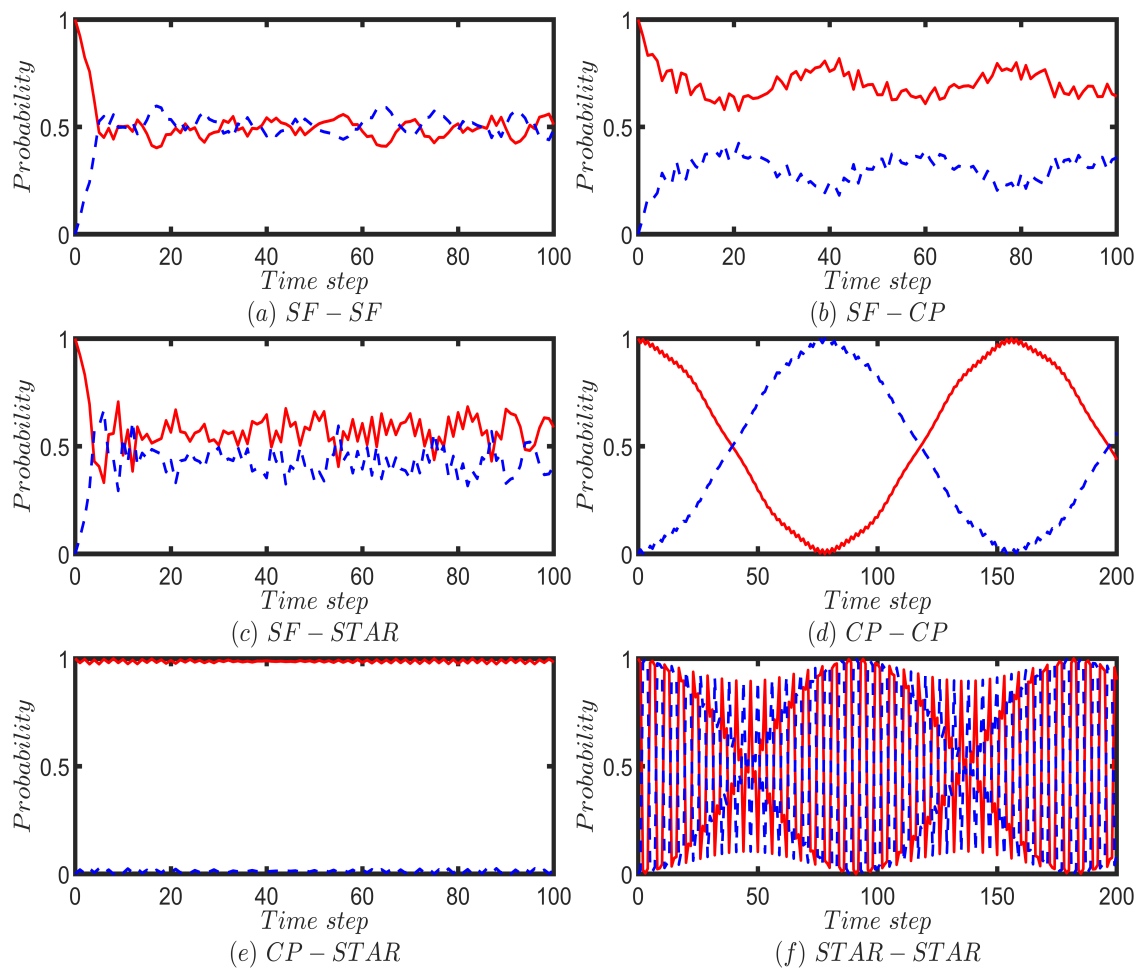


Figure 7. Illustrates the probability of finding the Grover walker on the top layer (red solid line) and the bottom layer (blue dotted line) of six different two-layered multiplex networks, each consisting of 100 nodes. The top and bottom layers of each multiplex network are constructed from combinations of scale-free (SF), complete (CP) and star networks with 50 nodes. For the case of SF-SF, two different scale-free networks are chosen. Grover walk is initiated from the localized position state of the form $|1\rangle_p \otimes \frac{1}{\sqrt{d_1}} \sum_{r=1}^{d_1} |f_1(r)\rangle_c$ and for each time step up to 100 steps, the probability of finding the walker on a given layer is calculated by summing the probabilities of finding the walker at each node corresponding to that layer. In cases (d,f), the time step has been extended to 200 steps to improve the clarity and visibility of the plot shapes.

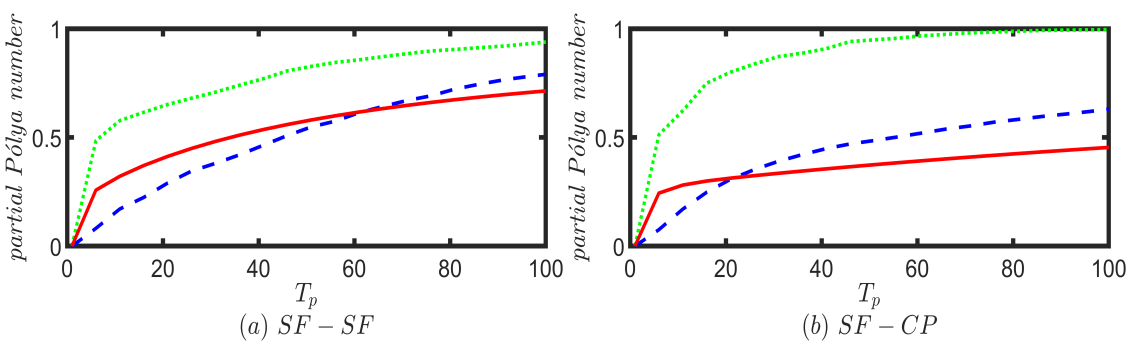


Figure 8. Cont.

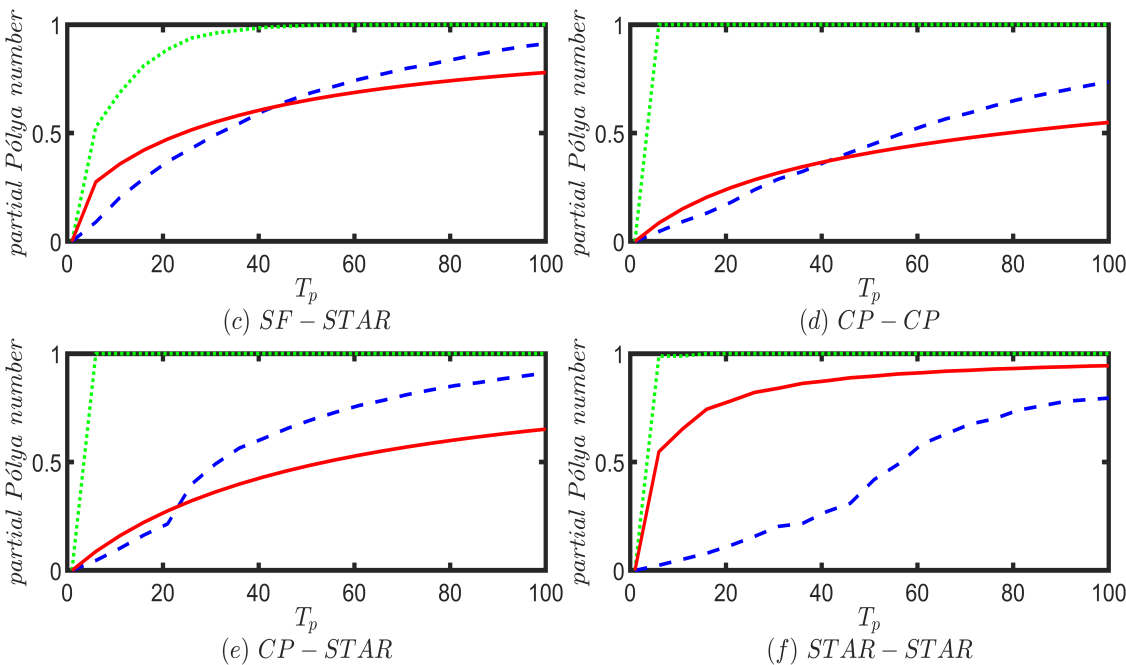


Figure 8. Convergence of the partial Pólya number for Grover (green dotted line), Fourier (blue dash line), and unbiased classical (red solid line) walkers on six different two-layered multiplex networks, each consisting of 100 nodes. The top and bottom layers of each multiplex network are constructed from combinations of scale-free (SF), complete (CP), and star networks with 50 nodes. For the case of SF-SF, two different scale-free networks are chosen. Partial Pólya number is calculated by choosing a set of finite time steps $T_p \in \{0, 5, 10, \dots, 100\}$ with a gap of 5 units. Each walk is initiated from node 1, and for both Grover and Fourier walks, the initial coin state is chosen as the uniform superposition of coin states.

7. Discussion

This article studied the dynamics of discrete-time quantum walks on multilayer networks. We derived a recurrence formula for the coefficients of the wave function of a quantum walker on an undirected graph with finite nodes. Then, by extending this formula to include extra layers, we developed a simulation to mimic the evolution of the quantum walker on a multilayer network. While multilayer networks have been studied in the context of CTQWs, to the best of our knowledge, there is a lack of literature related to the case of DTQWs. Hence, the prime objective of this study was to present a comprehensive mathematical framework to model DTQWs on multilayer networks with the aim of bridging this gap. In this regard, we employed our mathematical model to analyze the time-averaged probability and the return probability of the quantum walker on multilayer networks in relation to the Fourier and Grover walks. Moreover, we studied the impact of decoherence on the progression of Fourier walk on multilayer networks. For the sake of clarity and readability, first, we used a toy multilayer network to conduct our analysis. Later, we extended our analysis to much larger synthetic multilayer networks. Our study revealed that the Grover walk on a multilayer network exhibits rich dynamics. For instance, the Grover walker displays a periodic behavior of occupying the top and bottom layers of a two-layered multiplex network constructed from a complete graph or a star graph. Further research and analysis are essential to unlock the full potential of these insights for practical quantum applications, e.g., for quantum computation and quantum communication. Moreover, in relation to the recurrence probability, the Grover walker returns to the initial position faster than both Fourier and unbiased classical walkers. In the context of general QWs, the recurrence probability has a deep link to the localization property, playing a pivotal role in diverse applications, including quantum search algorithms and topological

insulators [36–39]. Hence, there seems to be significant potential for future studies related to the return probability on multilayer networks.

Another finding of this study is that the QWs on multilayer networks are vulnerable to decoherence arising from randomly broken links. Multilayer networks with a smaller number of nodes are sensitive to defects, even on a single edge. However, for larger multilayer networks, the tolerance of the QWs for decoherence appears to decrease as the number of broken links increases. Nonetheless, this observation should be further quantified and generalized in future research.

To experimentally realize quantum walks on multilayer networks, we need to implement a position-dependent coin. This can be achieved, e.g., by employing the method recently reported in [40]. In this experiment, a cascaded interferometric network was constructed incorporating birefringent calcite beam displacers to perform the conditional position shifts. Position-dependent coin operations were realized using various wave plates placed in the specific spatial modes of the heralded single photons traversing the setup.

As a future extension of this study, one could explore how other forms of decoherence models, such as Pauli channels, as well as amplitude and phase damping in the coin degree of freedom, impact the QWs on multilayer networks. In summary, we anticipate that the mathematical analysis we have performed here may have a profound influence on a broad spectrum of problems that can be modeled or assisted by DTQWs on multilayer networks.

Author Contributions: Conceptualization, M.N.J. and P.P.; methodology, M.N.J., P.P., D.B.P. and E.C.; software, M.N.J. and P.P.; validation, M.N.J., P.P., D.B.P. and E.C.; formal analysis, M.N.J., P.P., D.B.P. and E.C.; investigation, M.N.J., P.P., D.B.P. and E.C.; writing—original draft preparation, M.N.J.; writing—review and editing, P.P., D.B.P. and E.C.; visualization, M.N.J. and P.P.; supervision, E.C.; funding acquisition, E.C. All authors have read and agreed to the published version of the manuscript.

Funding: M. N. Jayakody acknowledges the President Scholarship Program at Bar-Ilan University. P. Pradhan acknowledges the Science and Engineering Research Board (SERB) grant TAR/2022/000657, Govt. of India. This research was funded in part by the Israeli Innovation Authority under Project No. 73795, by the Pazy Foundation, by the Israeli Ministry of Science and Technology, and by the Quantum Science and Technology Program of the Israeli Council of Higher Education.

Institutional Review Board Statement: Not applicable.

Data Availability Statement: The data and code can be made available upon request.

Conflicts of Interest: The authors declare no conflict of interest.

Appendix A. Arc-Reversal Model vs. Our Method Described in Section 2

In the realm of QWs, the arc-reversal model introduces a mechanism to reverse the direction of the walk along specific paths or arcs. This directional reversal aims to enhance interference effects, the constructive or destructive interaction of probability amplitudes, for different paths [17]. In the arc-reversal model, the state of the quantum walker is represented by a column vector. The global coin operator is defined by a block diagonal matrix where each block along the diagonal represents the local coin operators. The shifting operation is done by a permutation matrix, which is termed the arc-reversal matrix [17]. The size of the permutation and the coin matrices depend on the number of edges of the graph. With related to the numerical simulation of the arc-reversal model, a single step of the quantum walker's evolution is simulated by applying the coin matrix, followed by the permutation matrix, to the column vector that represents the current state of the quantum walker.

In our method, which is described in Section 2, we represent the state of the quantum walker as a block matrix, given in (9), rather than a column vector. In the abstract form of our model, we employ the same coin and shift operators as those used in the arc-reversal model (see Equations (5) and (6)). However, with related to the numerical simulation of our model, a single step of the quantum walker's evolution is simulated by updating the

elements of the block matrix that represent the state of the quantum walker and then by taking the transpose of the block matrix (see Equations (10) and (11)).

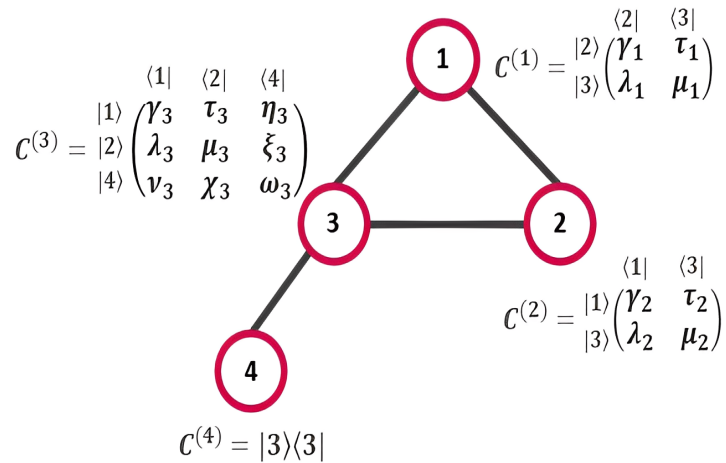


Figure A1. Graph of four vertexes and the coin operators associated with each vertex. For each vertex x , the elements of the coin operator associated to x are chosen in such a way that $C^{(x)}(C^{(x)})^\dagger = (C^{(x)})^\dagger C^{(x)} = \mathbb{I}$ where $x \in \{1, 2, 3, 4\}$.

Hence, in our method, the coin operation is performed by updating the elements of the block matrix, and the shifting operation is performed by taking the transpose of the block matrix that represents the state of the quantum walker. Moreover, in our model, the size of the block matrix N_t , which we use to represent the state of the quantum walker, depends on the number of vertices of the graph. Hence, whenever the number of vertices is less than the number of edges, our method could be more memory efficient than the arc-reversal model (the arc-reversal model requires much bigger matrices than ours). Further, we can explain the difference between the arc-reversal model and our method by referring to the following example. Let us consider the graph given in Figure A1. The corresponding set of vertices and edges can be written as $V = \{|1\rangle_p, |2\rangle_p, |3\rangle_p, |4\rangle_p\}$ and $E = \{\{1, 2\}, \{1, 3\}, \{2, 1\}, \{2, 3\}, \{3, 1\}, \{3, 2\}, \{3, 4\}, \{4, 3\}\}$ respectively. Now let us define the sets of B_x as follows; $B_1 = \{2, 3\}$, $B_2 = \{1, 3\}$, $B_3 = \{1, 2, 4\}$ and $B_4 = \{3\}$. The function $f_x(r)$ (r th element of the B_x set) can be defined as follows; $f_1(1) = 2$, $f_1(2) = 3$; $f_2(1) = 1$, $f_2(2) = 3$; $f_3(1) = 1$, $f_3(2) = 2$, $f_3(3) = 4$ and $f_4(1) = 3$. Then, the state vector of the quantum walker at time t can be written as

$$|\psi_t\rangle = \sum_{x=1}^4 \sum_{r=1}^{d_x} \alpha_{x,f_x(r)}(t) |x\rangle_p |f_x(r)\rangle_c \quad (\text{A1})$$

The state vector given in (A1) can be represented in terms of the block matrix N_t as

$$N_t = \begin{pmatrix} |1\rangle_c & |2\rangle_c & |3\rangle_c & |4\rangle_c \\ |1\rangle_p \left(\begin{array}{cccc} 0 & \alpha_{1,2}(t) & \alpha_{1,3}(t) & 0 \\ \alpha_{2,1}(t) & 0 & \alpha_{2,3}(t) & 0 \\ \alpha_{3,1}(t) & \alpha_{3,2}(t) & 0 & \alpha_{3,4}(t) \\ 0 & 0 & \alpha_{4,3}(t) & 0 \end{array} \right) & |2\rangle_p \\ |3\rangle_p & |4\rangle_p \end{pmatrix} \quad (\text{A2})$$

Note that, by updating the elements of N_t using the relationships given in (10) and (11), one can mimic the evolution of a QW on the graph in Figure A1. However, according to the arc-reversal model [17], matrices with the size of 8×8 are used to represent the permutation (R_{arc}) and coin (C_{arc}) matrices related to the graph in Figure A1 as given below

$$\mathbf{R}_{arc} = \begin{pmatrix} & (1,2) & (1,3) & (2,1) & (2,3) & (3,1) & (3,2) & (3,4) & (4,3) \\ (1,2) & 0 & 0 & 1 & 0 & 0 & 0 & 0 & 0 \\ (1,3) & 0 & 0 & 0 & 0 & 1 & 0 & 0 & 0 \\ (2,1) & 1 & 0 & 0 & 0 & 0 & 0 & 0 & 0 \\ (2,3) & 0 & 0 & 0 & 0 & 0 & 1 & 0 & 0 \\ (3,1) & 0 & 1 & 0 & 0 & 0 & 0 & 0 & 0 \\ (3,2) & 0 & 0 & 0 & 1 & 0 & 0 & 0 & 0 \\ (3,4) & 0 & 0 & 0 & 0 & 0 & 0 & 0 & 1 \\ (4,3) & 0 & 0 & 0 & 0 & 0 & 0 & 1 & 0 \end{pmatrix} \quad (A3)$$

$$\mathbf{C}_{arc} = \begin{pmatrix} \mathcal{C}^{(1)} & 0 & 0 & 0 \\ 0 & \mathcal{C}^{(2)} & 0 & 0 \\ 0 & 0 & \mathcal{C}^{(3)} & 0 \\ 0 & 0 & 0 & \mathcal{C}^{(4)} \end{pmatrix} \quad (A4)$$

Moreover, a column vector with the size of 8×1 represents the state of the walker. Nonetheless, our method uses a 4×4 matrix to represent the same graph in Figure A1. Furthermore, in the arc reversal model, the position and coin states are not explicitly represented. But in our method, we explicitly represent the position, and the coin states as a tensor product.

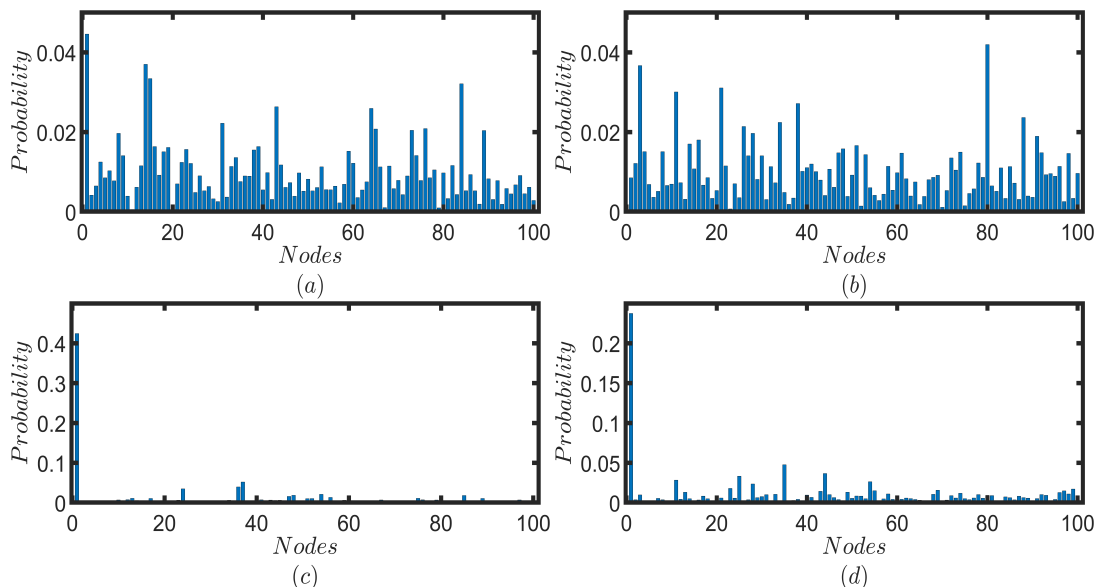


Figure A2. Probability distributions of the Fourier and Grover walk after 100 time steps on a two-layered multiplex network. The top and bottom layers of the multiplex network comprise two different Erdős-Rényi (ER) networks, each with 50 nodes. Subfigures (a,c) show the probability profiles of the Fourier and Grover walks on the entire network, respectively. Subfigure (b) displays the probability profile when the Fourier and Grover coins are attached to the top and bottom layers. Subfigure (d) presents the probability profile when the Grover and Fourier coins are attached to the top and bottom layers. Both walks are initiated from the localized state of $|1\rangle_p \otimes |f_1(1)\rangle_c$.

Appendix B. Coin Flip and Shift Operation

Proof. Let us represent the state vector $|\psi_t\rangle$ given by (3) in the block matrix form. That is $|\psi_t\rangle \equiv \mathbf{N}_t$. Now let us apply the global coin operator C given in (5) on the total wave function $|\psi_t\rangle$ in (3). Then we get the following expression

$$C|\psi_t\rangle = \sum_{x=1}^n \sum_{i=1}^{d_x} \left(\sum_{j=1}^{d_x} \alpha_{x,f_x(j)}(t) C_{ij}^{(x)} \right) |x\rangle_p |f_x(i)\rangle_c \quad (A5)$$

Let us write $\tilde{\alpha}_{x,f_x(i)}(t) = \left(\sum_{j=1}^{d_x} \alpha_{x,f_x(j)}(t) C_{ij}^{(x)}\right)$. Then we can rewrite (A5) as follows

$$C|\psi_t\rangle = \sum_{x=1}^n \sum_{i=1}^{d_x} \tilde{\alpha}_{x,f_x(i)}(t) |x\rangle_p |f_x(i)\rangle_c \quad (\text{A6})$$

Note that $C|\psi_t\rangle$ can also be represented in the block matrix form. Let us denote $C|\psi_t\rangle \equiv \tilde{\mathbf{N}}_t$. Now let us apply the shift operator S given in (6) on $C|\psi_t\rangle$. The result can be written as

$$SC|\psi_t\rangle = \sum_{x=1}^n \sum_{i=1}^{d_x} \tilde{\alpha}_{x,f_x(i)}(t) |f_x(i)\rangle_p |x\rangle_c \quad (\text{A7})$$

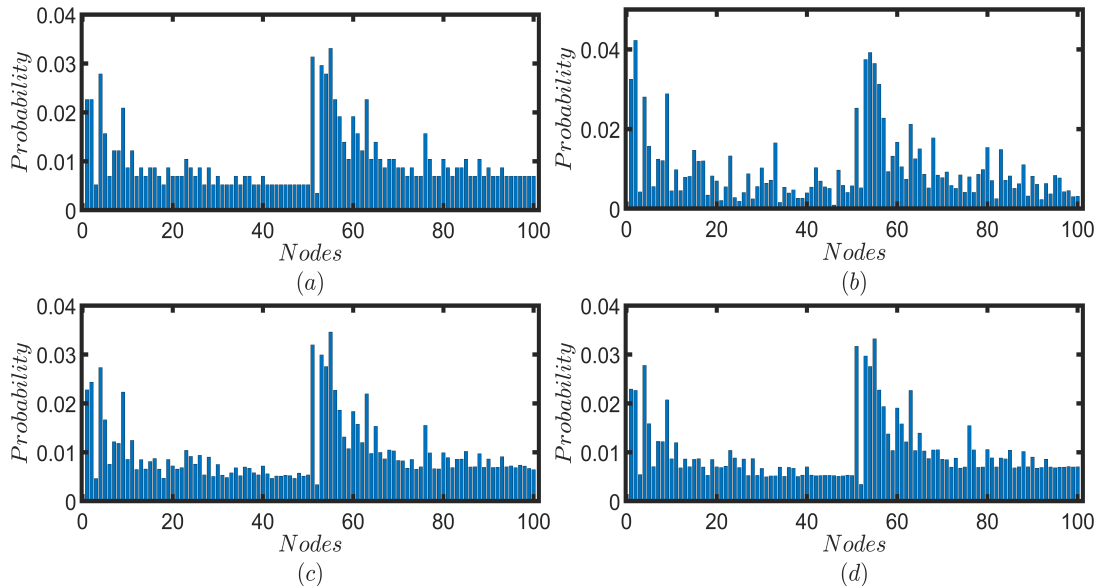


Figure A3. Probability distributions of the (a) unbiased CRW and (b) the standard Fourier walk after 100 time steps on the two-layered multiplex network. The average probability distributions of the Fourier walk subjected to a single $(1, f_1(1))$ and seven $\{(x, f_x(1))\}_{x \in W}$ broken links where $W = \{1, 10, 30, 40, 50, 60, 80\}$ are given in (c,d), respectively. The top and bottom layers of the multiplex network comprise two different scale-free (SF) networks, each with 50 nodes. The unbiased CRW is initiated from node 1, and the Fourier walk is initiated from the localized state of $|1\rangle_p \otimes |f_1(1)\rangle_c$. The average probability distributions are generated by breaking some intralayer edgers of the SF-SF multilayer network with a 0.5 probability at each time step of the Fourier walk and by averaging over 1000 trials.

Let the block matrix form of $SC|\psi_t\rangle$ be \mathbf{M}_t . By observing (A6) and (A7) one can argue that the elements in the x th row of $\tilde{\mathbf{N}}_t$ is equal to the elements in the x th column of \mathbf{M}_t . That is, \mathbf{M}_t is equal to the transpose of $\tilde{\mathbf{N}}_t$. In addition, we have the following expression

$$SC|\psi_t\rangle = |\psi_{t+1}\rangle = \sum_{x=1}^n \sum_{i=1}^{d_x} \alpha_{x,f_x(i)}(t+1) |x\rangle_p |f_x(i)\rangle_c \quad (\text{A8})$$

Thus, for each $x \in \{1, \dots, n\}$ and $r \in \{1, \dots, d_x\}$ we can derive a recurrence relationship between the elements of \mathbf{N}_t and \mathbf{N}_{t+1} as follows

$$\alpha_{x,f_x(r)}(t+1) = \tilde{\alpha}_{f_x(r),x}(t) \quad (\text{A9})$$

This completes the proof. \square

Appendix C. Some Probability Profiles of UBCRW, Fourier and Grover Walks

Figure A2 depicts the probability profiles of QWs performed on a two-layered multiplex network in which each layer possesses a different coin. The walker is initiated from a randomly chosen node. According to Figure A2, one can easily identify that the impact of the coin operator used on the top layer, from which the walk is initiated, becomes dominant over the whole multilayer network irrespective of the coin operator used in the bottom layer.

Figure A3 presents the probability profiles of the unbiased CRW, the standard Fourier walk, and the Fourier walk subjected to the broken links decoherence model on two-layer multiplex networks. By comparing the probability profile of the unbiased CRW (Figure A3a) with the mean probability distributions of the Fourier walk subjected decoherence (Figure A3c,d), one can observe that, Figure A3a,d closely resemble each other more than Figure A3a,c.

Appendix D. Probability Profiles of UBCRW on Six Different Multiplex Networks

Figure A4 shows the probability of finding the unbiased classical walker on six different synthetic two-layered multiplex networks with 100 nodes.

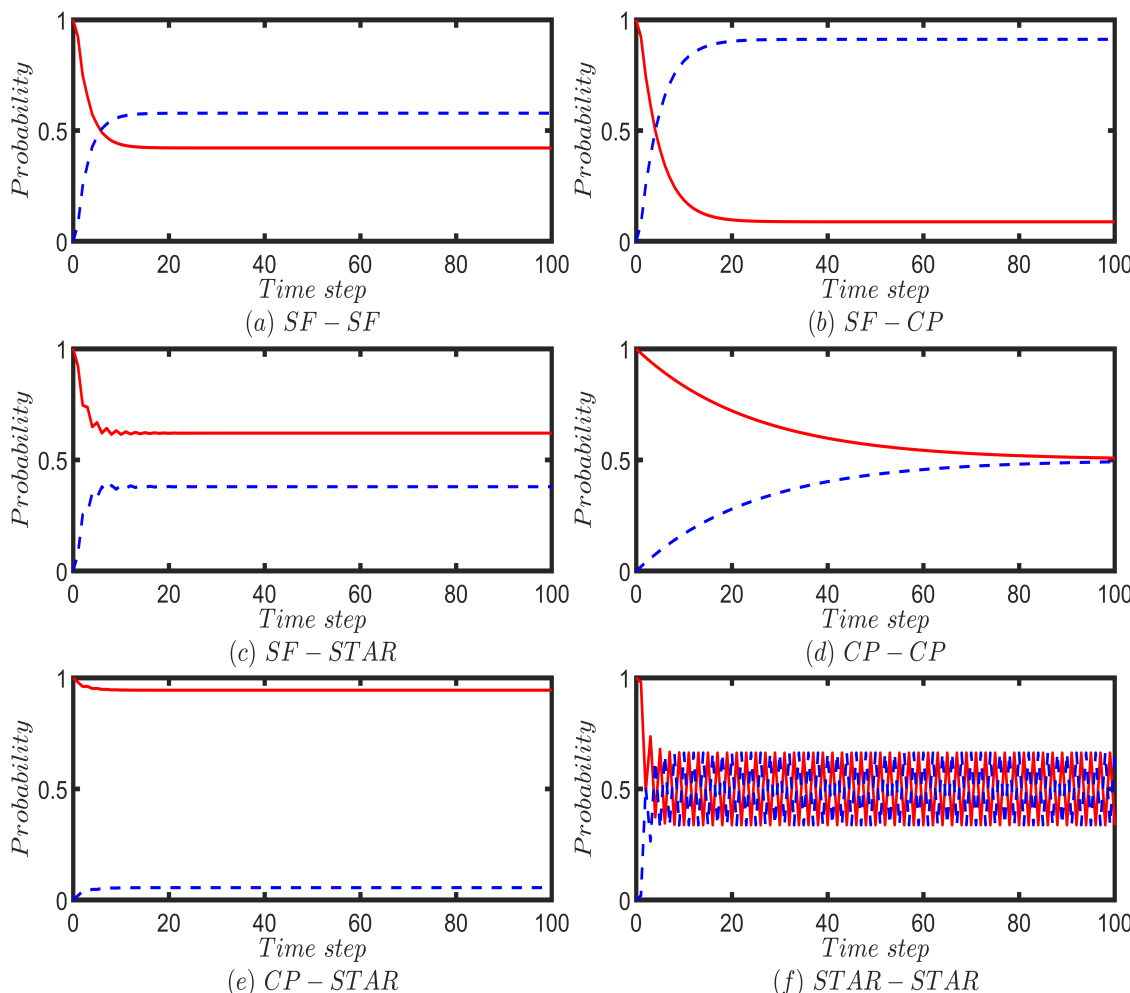


Figure A4. Illustrates the probability of finding the unbiased classical walker on the top layer (red solid line) and the bottom layer (blue dotted line) of six different two-layered multiplex networks, each consisting of 100 nodes. The top and bottom layers of each multiplex network are constructed from combinations of scale-free (SF), complete (CP), and star networks with 50 nodes. For the case of SF-SF, two different scale-free networks are chosen. The UBCRW is initiated from vertex 1, and for each time step up to 100 steps, the probability of finding the walker on a given layer is calculated by summing the probabilities of finding the walker at each node corresponding to that layer.

References

- Childs, A.M.; Gosset, D.; Webb, Z. Universal computation by multiparticle quantum walk. *Science* **2013**, *339*, 791–794. [[CrossRef](#)] [[PubMed](#)]
- Kempe, J. Quantum random walks: An introductory overview. *Contemp. Phys.* **2003**, *44*, 307–327. [[CrossRef](#)]
- Wang, J.; Manouchehri, K. *Physical Implementation of Quantum Walks*; Springer: Berlin/Heidelberg, Germany, 2013.
- Venegas-Andraca, S.E. Quantum walks: A comprehensive review. *Quantum Inf. Process.* **2012**, *11*, 1015–1106. [[CrossRef](#)]
- Aleta, A.; Moreno, Y. Multilayer networks in a nutshell. *Annu. Rev. Condens. Matter Phys.* **2019**, *10*, 45–62. [[CrossRef](#)]
- Jalan, S.; Pradhan, P. Localization of multilayer networks by optimized single-layer rewiring. *Phys. Rev. E* **2018**, *97*, 042314. [[CrossRef](#)]
- De Domenico, M.; Granell, C.; Porter, M.A.; Arenas, A. The physics of spreading processes in multilayer networks. *Nat. Phys.* **2016**, *12*, 901–906. [[CrossRef](#)]
- Pilosof, S.; Porter, M.A.; Pascual, M.; Kéfi, S. The multilayer nature of ecological networks. *Nat. Ecol. Evol.* **2017**, *1*, 0101. [[CrossRef](#)] [[PubMed](#)]
- Gosak, M.; Markovič, R.; Dolenšek, J.; Rupnik, M.S.; Marhl, M.; Stožer, A.; Perc, M. Network science of biological systems at different scales: A review. *Phys. Life Rev.* **2018**, *24*, 118–135. [[CrossRef](#)]
- Gallotti, R.; Barthélémy, M. The multilayer temporal network of public transport in Great Britain. *Sci. Data* **2015**, *2*, 140056. [[CrossRef](#)]
- Musmeci, N.; Nicosia, V.; Aste, T.; Di Matteo, T.; Latora, V. The multiplex dependency structure of financial markets. *Complexity* **2017**, *2017*, 9586064. [[CrossRef](#)]
- Galiceanu, M.; Strunz, W.T. Continuous-time quantum walks on multilayer dendrimer networks. *Phys. Rev. E* **2016**, *94*, 022307. [[CrossRef](#)] [[PubMed](#)]
- Maquiné Batalha, G.; Volta, A.; Strunz, W.T.; Galiceanu, M. Quantum transport on honeycomb networks. *Sci. Rep.* **2022**, *12*, 6896. [[CrossRef](#)] [[PubMed](#)]
- Maciel, C.M.; Mendes, C.F.; Strunz, W.T.; Galiceanu, M. Quantum transport on generalized scale-free networks. *Phys. Rev. A* **2020**, *102*, 032219. [[CrossRef](#)]
- Ambainis, A. Quantum walks and their algorithmic applications. *Int. J. Quantum Inf.* **2003**, *1*, 507–518. [[CrossRef](#)]
- Aharonov, D.; Ambainis, A.; Kempe, J.; Vazirani, U. Quantum walks on graphs. In Proceedings of the Thirty-Third Annual ACM Symposium on Theory of Computing, Hersonissos, Greece, 6 July 2001; pp. 50–59.
- Godsil, C.; Zhan, H. Discrete-time quantum walks and graph structures. *J. Comb. Theory Ser. A* **2019**, *167*, 181–212. [[CrossRef](#)]
- Watrous, J. Quantum simulations of classical random walks and undirected graph connectivity. *J. Comput. Syst. Sci.* **2001**, *62*, 376–391. [[CrossRef](#)]
- Kendon, V. Quantum walks on general graphs. *Int. J. Quantum Inf.* **2006**, *4*, 791–805. [[CrossRef](#)]
- Feldman, E.; Hillery, M. Scattering theory and discrete-time quantum walks. *Phys. Lett. A* **2004**, *324*, 277–281. [[CrossRef](#)]
- Jayakody, M.N.; Meena, C.; Pradhan, P. Revisiting one-dimensional discrete-time quantum walks with general coin. *Phys. Open* **2023**, *17*, 100189. [[CrossRef](#)]
- Manouchehri, K.; Wang, J. Quantum random walks without walking. *Phys. Rev. A* **2009**, *80*, 060304. [[CrossRef](#)]
- Boccaletti, S.; Bianconi, G.; Criado, R.; Del Genio, C.I.; Gómez-Gardenes, J.; Romance, M.; Sendina-Nadal, I.; Wang, Z.; Zanin, M. The structure and dynamics of multilayer networks. *Phys. Rep.* **2014**, *544*, 1–122. [[CrossRef](#)]
- Mukai, K.; Hatano, N. Discrete-time quantum walk on complex networks for community detection. *Phys. Rev. Res.* **2020**, *2*, 023378. [[CrossRef](#)]
- Al-sharoa, E.; Aviyente, S. A Unified Spectral Clustering Approach for Detecting Community Structure in Multilayer Networks. *Symmetry* **2023**, *15*, 1368. [[CrossRef](#)]
- Lovász, L. Random walks on graphs. *Comb. Paul Erdos Is Eighty* **1993**, *2*, 4.
- Venegas-Andraca, S.E. *Quantum Walks for Computer Scientists*; Morgan and Claypool Publishers: San Rafael, CA, USA, 2008; Volume 1, pp. 1–119.
- Baptista, A.; Gonzalez, A.; Baudot, A. Universal multilayer network exploration by random walk with restart. *Commun. Phys.* **2022**, *5*, 170. [[CrossRef](#)]
- Gomez, S.; Diaz-Guilera, A.; Gomez-Gardenes, J.; Perez-Vicente, C.J.; Moreno, Y.; Arenas, A. Diffusion dynamics on multiplex networks. *Phys. Rev. Lett.* **2013**, *110*, 028701. [[CrossRef](#)] [[PubMed](#)]
- Faccin, M.; Johnson, T.; Biamonte, J.; Kais, S.; Migdał, P. Degree distribution in quantum walks on complex networks. *Phys. Rev. X* **2013**, *3*, 041007. [[CrossRef](#)]
- Pólya, G. Über eine Aufgabe der Wahrscheinlichkeitsrechnung betreffend die Irrfahrt im Straßennetz. *Math. Ann.* **1921**, *84*, 149. [[CrossRef](#)]
- Štefaňák, M.; Kiss, T.; Jex, I. Recurrence properties of unbiased coined quantum walks on infinite d -dimensional lattices. *Phys. Rev. A* **2008**, *78*, 032306. [[CrossRef](#)]
- Štefaňák, M.; Jex, I.; Kiss, T. Recurrence and Pólya number of quantum walks. *Phys. Rev. Lett.* **2008**, *100*, 020501. [[CrossRef](#)]
- Leung, G.; Knott, P.; Bailey, J.; Kendon, V. Coined quantum walks on percolation graphs. *New J. Phys.* **2010**, *12*, 123018. [[CrossRef](#)]
- Kollár, B.; Kiss, T.; Novotný, J.; Jex, I. Asymptotic dynamics of coined quantum walks on percolation graphs. *Phys. Rev. Lett.* **2012**, *108*, 230505. [[CrossRef](#)] [[PubMed](#)]

36. Kiumi, C.; Konno, N.; Tamura, S. Return probability of quantum and correlated random walks. *Entropy* **2022**, *24*, 584. [[CrossRef](#)] [[PubMed](#)]
37. Sajid, M.; Asbóth, J.K.; Meschede, D.; Werner, R.F.; Alberti, A. Creating anomalous Floquet Chern insulators with magnetic quantum walks. *Phys. Rev. B* **2019**, *99*, 214303. [[CrossRef](#)]
38. Kitagawa, T.; Rudner, M.S.; Berg, E.; Demler, E. Exploring topological phases with quantum walks. *Phys. Rev. A* **2010**, *82*, 033429. [[CrossRef](#)]
39. Khazali, M. Discrete-time quantum-walk & Floquet topological insulators via distance-selective Rydberg-interaction. *Quantum* **2022**, *6*, 664.
40. Wang, X.; Zhan, X.; Li, Y.; Xiao, L.; Zhu, G.; Qu, D.; Lin, Q.; Yu, Y.; Xue, P. Generalized Quantum Measurements on a Higher-Dimensional System via Quantum Walks. *Phys. Rev. Lett.* **2023**, *131*, 150803. [[CrossRef](#)]

Disclaimer/Publisher’s Note: The statements, opinions and data contained in all publications are solely those of the individual author(s) and contributor(s) and not of MDPI and/or the editor(s). MDPI and/or the editor(s) disclaim responsibility for any injury to people or property resulting from any ideas, methods, instructions or products referred to in the content.